Optics Letters

On-chip silicon photonic integrated frequency-tunable bandpass microwave photonic filter

Weifeng Zhang and Jianping Yao*

Microwave Photonic Research Laboratory, School of Electrical Engineering and Computer Science, University of Ottawa, 800 King Edward Avenue, Ottawa, Ontario K1 N 6N5, Canada
**Corresponding author: jpyao@eecs.uottawa.ca*

Received 21 May 2018; revised 27 June 2018; accepted 27 June 2018; posted 2 July 2018 (Doc. ID 332244); published 24 July 2018

An on-chip frequency-tunable bandpass microwave photonic filter (MPF) implemented on a silicon photonic platform is reported. The on-chip MPF consists of a high-speed phase modulator (PM), a thermally tunable high-*Q* micro-disk resonator (MDR), and a high-speed photodetector (PD). The filtering function of the MPF is realized based on phase modulation and phase modulation to intensity modulation conversion, to translate the spectral response of the MDR in the optical domain to the spectral response of the MPF in the microwave domain. The tunability of the MPF is realized by thermally tuning the MDR. The proposed on-chip bandpass MPF is fabricated and characterized. An MPF with a passband of 1.93 GHz and a tunable range from 3 to 10 GHz is demonstrated. The power consumption, the insertion loss, and the bandwidth over the entire tunable range are studied. This successful implementation of an MPF marks a significant step forward in the full integration of microwave photonic systems on a single chip.

OCIS codes: (130.3120) Integrated optics devices; (120.2440) Filters; (140.4780) Optical resonators; (350.4010) Microwaves.

https://doi.org/10.1364/OL.43.003622

With an exponential increase in data traffic, microwave carrier frequencies for wireless communications have been increasing to meet the bandwidth requirements. Consequently, microwave signal processing at a high-frequency band is becoming an important issue. As one of the fundamental processing functions, microwave filtering at a high frequency with a large frequency tunable range is urgently needed. Thanks to the development of modern photonics, microwave filters implemented based on photonic components are considered to be a key solution to overcome the challenge [1,2]. In the past 20 years, great efforts have been directed to the study of microwave filters based on photonics, and numerous solutions have been proposed [3,4]. In general, microwave photonic filters (MPFs) can be implemented, either in the incoherent or coherent regime. For an incoherent MPF, a delay-line configuration with a finite-impulse response or infinite-impulse response is used [5–7]. For a coherent filter, an optical filter is used to translate the spectral response of the optical filter from the optical domain to the microwave domain [8,9]. Compared with an incoherent MPF, a coherent MPF usually has a simpler configuration which is a desired feature for photonic integration.

Most of the MPFs proposed in the past are implemented based on discrete photonic components, making the filters very bulky, expensive, and high-power consuming. For many applications, it is highly desirable that an MPF is implemented using a photonic integrated circuit [10]. Recently, a monolithically integrated MPF on an indium phosphide (InP) substrate has been demonstrated [11]. In its implementation, all elements, including a laser source, a modulator, an optical filter, and a photodetector (PD), are integrated on a single chip. By controlling electrical currents into the micro-heaters to tune the optical filter, the MPF is tuned. The main problems associated with the InP-based MPF implementation are the large size, high loss, and high fabrication cost. In addition, the difficulty in achieving seamless integration with electronics is another problem that is hard to solve [12]. In the contrast, silicon photonics, a material system that exhibits overwhelming advantages in terms of the footprint, loss, and fabrication cost, has been extensively studied for microwave photonic integration. The compatibility with a mature CMOS process is another overwhelming advantage that makes it possible for low-cost and seamless integration with electronics [13].

Recently, we reported an integrated MPF implemented on a silicon photonic platform [14,15]. The integrated MPF includes three key components: a high-speed phase modulator (PM), a thermally tunable high-*Q* micro-disk resonator (MDR), and a high-speed PD. With an external light wave injected into the chip, the PM, the MDR, and the PD are operating jointly to form a bandpass MPF, realized based on phase modulation and phase modulation to intensity modulation (PM-IM) conversion. By controlling the electrical power applied to the metallic micro-heater located on top of the MDR, the resonance frequency of the resonator is tuned due to thermal-optic effect. As a result, the central frequency of the MPF is tuned. Furthermore, with the same design chip, we also demonstrated a frequency-tunable opto-electrical oscillator for microwave signal generation in Ref. [16].

The work reported in this Letter is an extension of our earlier work reported in Refs. [14,15]. Here, a more detailed study, including the power consumption, the microwave loss, and the

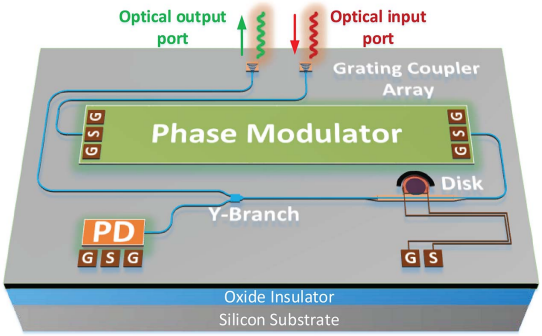

Fig. 1. Perspective view of the proposed integrated MPF on a silicon photonic chip.

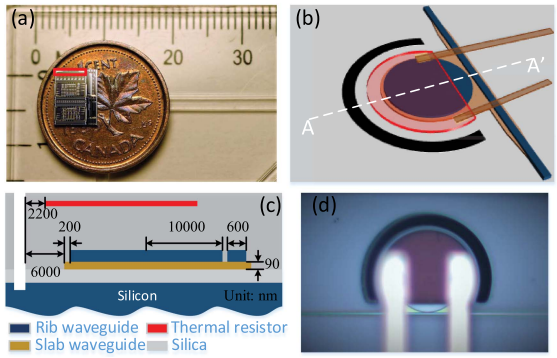

Fig. 2. (a) Image of the fabricated silicon photonic chip captured by a microscope camera, (b) schematic view of the designed thermally tunable high-Q MDR, (c) cross-sectional view of the MDR with a top-placed micro-heater, and (d) image of the tunable MDR in the fabricated chip.

bandwidth over the entire tuning range is performed. The proposed on-chip bandpass MPF has a bandwidth of 1.93 GHz with a tunable range of 7 GHz, from 3 to 10 GHz. The successful demonstration of this silicon photonic MPF represents a significant step forward in the full integration of a microwave photonic subsystem or system on a single silicon photonic chip, which opens up new avenues toward real applications of microwave photonic systems.

Figure 1 illustrates the perspective view of the proposed MPF. It consists of a high-speed PM, a thermally tunable high-Q MDR, and a high-speed PD. A CW light from an external laser diode (LD) is coupled into the chip via an input grating coupler. In order to minimize the chip size, a single-mode strip waveguide structure is mostly used to route the optical signal within the chip. The input CW light is first guided to the high-speed PM, where the incoming microwave signal to be processed is modulated on the optical carrier. A phase-modulated optical signal is generated at the output of the PM, which is sent to the high-Q MDR where PM-IM conversion is performed [9]. A compact Y-branch coupler is connected to the output of the MDR to split the optical signal equally into two channels. One channel of the optical signal is sent to the high-speed PD, where optical-to-electrical conversion is performed to recover the filtered microwave signal, and the other channel is routed to an output grating coupler to couple the light out of the chip, to enable real-time monitoring of the optical spectrum by an optical spectrum analyzer (OSA). For the optical I/O coupling, the input and output grating couplers are deployed with a center-to-center spacing of 127 μm, which is equal to the physical spacing between two adjacent fibers in the fiber array. If the phase-modulated optical signal is applied to the PD directly, due to the out-of-phase nature of the upper and lower sidebands, the beating between the upper sideband and the optical carrier will fully cancel the beating between the lower sideband and the optical carrier; thus, no microwave signal will be generated at the output of the PD. In our proposed MPF, if one of the two sidebands of the phase-modulated optical signal falls in the notch of the MDR, only one beat signal is generated, and the phase-modulated signal is converted to a single-sideband intensity-modulated signal, and a microwave signal is obtained at the output of the PD. The entire operation corresponds to a microwave bandpass filter with the spectral response of the microwave filter being translated from the spectral response of the optical notch filter. The configuration of the proposed MPF is very simple, which is advantageous to ensure the MPF to have a small footprint and a small optical insertion loss.

The proposed integrated MPF is fabricated using a CMOS-compatible process with 248 nm deep ultraviolet lithography. Figure 2(a) gives an image of the fabricated MPF captured by a microscope camera, in which the red line outlines the area of the MPF. In the implementation, the high-speed PM is designed to have a travelling wave structure. A lateral pn junction is produced in the rib waveguide to realize high-speed modulation based on the free-carrier plasma dispersion effect in silicon. When a reverse bias voltage of 4 V is applied to the PM, the PM is measured to have a 3 dB modulation bandwidth as large as 20.85 GHz. The high-speed PIN PD is implemented by doping the PD waveguide with germanium. When a reverse bias voltage of 7.5 V is applied, the PD is measured to have a 3 dB bandwidth of 15.69 GHz.

Since the spectral response of the optical notch filter determines the spectral response of the MPF, in the proposed MPF, the MDR, serving as an optical filter, is a critical component. Figure 2(b) shows the perspective view of the MDR with an all-pass configuration. The radius of the MDR is 10 μm. Since the frequency response of the MPF is translated from the spectral response of the MDR, to have a narrow passband, an MDR with a high Q-factor is essential. To increase the Q-factor, the MDR is specifically designed to incorporate an additional slab waveguide to wrap the disk and the lateral sides of the bus waveguide, as shown in Fig. 2(b), to decrease the scattering loss of the confined optical field due to the disk sidewall roughness, to make the MDR have a larger Q-factor and to enhance the optical coupling between the disk and the bus waveguides [17]. Figure 2(c) presents the cross-sectional view of the MDR along the white dashed line AA' in Fig. 2(b). The disk and the bus waveguide have a height of 220 nm, and the slab waveguide has a height of 90 nm. The widths of the slab waveguide around the disk and the bus waveguide are 200 nm and, in the coupling region, the two slab waveguides overlap fully. To meet the phase-matching condition, the width of the bus waveguide is 600 nm to effectively excite the first-order whispering gallery mode (WGM). Thanks to the high thermo-optic coefficient in silicon, the MDR is designed to be thermally tunable which is done by incorporating a metallic micro-heater on top of the disk. To avoid the thermal impact on neighboring components

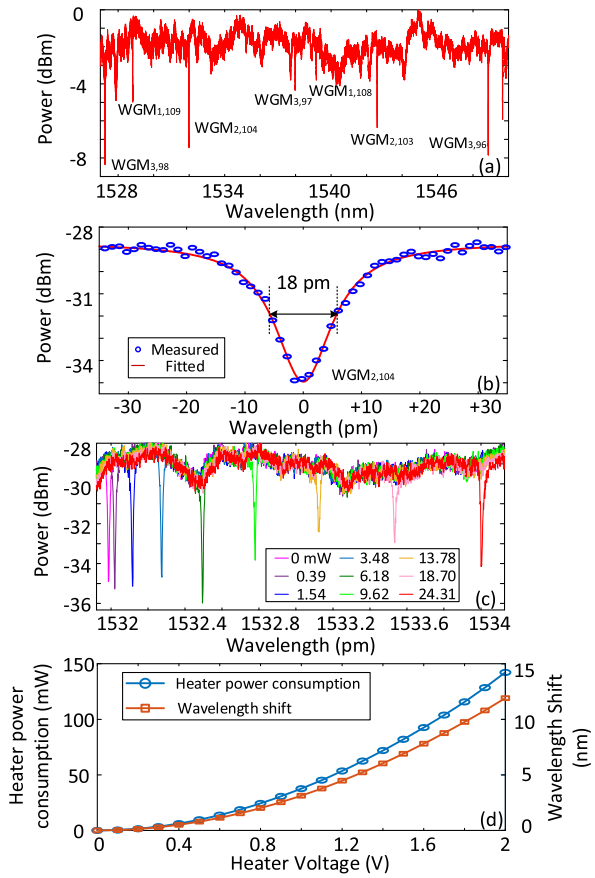

Fig. 3. (a) Measured transmission spectrum of the fabricated MDR, (b) zoom-in view of the $WGM_{2,104}$, (c) spectrum tuning of the MDR with a DC current applied to the micro-heater, and (d) power consumption of the heater and resonance wavelength shift when the voltage applied to the heater is increasing.

in the chip, a deep trench with a distance of 2.2 μm away from the micro-heater is etched around the disk for thermal isolation.

Then the optical performance of the MDR is evaluated, which is done by using an optical vector analyzer (LUNA OVA CTe). Figure 3(a) shows the measured transmission spectrum of the fabricated MDR. As can be seen, the MDR has the first-, second-, and third-order WGMs. The first-order WGM is measured to have a free spectral range (FSR) of 10.4 nm, the second-order WGM has an FSR of 10.6 nm, and the third-order WGM has an FSR of 10.7 nm. Figure 3(b) shows the zoom-in view of the resonance $WGM_{2,104}$ at 1531.99 nm and its Lorentzian fitting. A 3 dB bandwidth of 18 pm is measured, corresponding to a Q-factor of around 0.85×10^5, with an extinction ratio of 5.8 dB. Figure 3(c) shows that the spectrum of the MDR by increasing the DC current applied to the micro-heater. From the voltage-current measurement, the micro-heater resistance is estimated to be 25.5 Ω. When a DC current is applied to the micro-heater, due to the thermal-optic effect, the refractive index of the silicon is increased, and, thus, the resonance wavelength of the MDR is red shifted. As can be seen in Fig. 3(c), with the micro-heater power increasing from 0 to 24.31 mW, the resonance wavelength of the MDR is red shifted by 2.03 nm. During the red shift, the extinction ratio of the notch is changed, which is caused by the waveguide-dispersion-induced coupling condition change for different optical wavelengths. Figure 3(d) shows the heater power consumption and resonance wavelength shift of the MDR with the voltage applied to the micro-heater being increased continuously. When the applied electrical power is 128.52 mW, the red-shift amount of the notch is 10.87 nm, which is larger than one FSR. The wavelength shift rate is calculated to be 68.6 pm/mW. The key advantages of using the MDR in the implementation of the MPF include a high Q-factor and a strong thermal tunability with ultra-low power consumption.

An experiment is performed to evaluate the on-chip MPF. Figure 4(a) shows the experimental set-up. Since the chip has a high-level integration, the experimental setup is very simple with only an external LD and polarization controller (PC) needed to complete the system. The LD is used to generate a CW light with a wavelength of 1532.01 nm and a power of 8 dBm, and the PC is used to manage the state of polarization of the input light. A vector network analyzer (VNA) [Keysight N5227A] is employed to measure the frequency response of the MPF. A microwave signal generated from the VNA with a frequency tuned from 2 to 10 GHz and a constant power of 10 dBm is applied to the PM. At the optical output grating coupler, an OSA is used to real-time monitor the optical spectrum of the optical signal from the MDR. Three bias voltages provided by three high-precision voltage source meters (Keithley 2400) are applied to the PM, the MDR, and the PD. Figure 4(b) is a picture showing a fiber array and a microwave probe setup captured by a camera. The fiber array is used to couple the CW light from the LD into the chip and to couple the optical signal from the MDR out of the chip. A ground-signal-ground (GSG) microwave probe is connected to the microwave port of the PM in combination with a bias tee, to apply the microwave signal from the VNA together with a reverse bias voltage to the PM. At the end of the PM, a matched impedance terminator is connected to reduce the microwave signal reflection. The microwave signal at the output of the PD is connected by a GSG microwave probe in combination with another bias tee. For thermal tuning of the MDR, a DC probe is used to apply a DC current to the MDR. Note that, due to the very close proximity of the probes, free-space coupling between the microwave probes would happen, especially at higher frequencies, which limits the frequency tuning range of the MPF. The free-space coupling can be reduced if the chip is well packaged.

Figure 5(a) shows the measured frequency response when the MPF has a center frequency of 5.84 GHz with a DC current having a power of 0.33 mW applied to the micro-heater. This MPF is measured to have a 3 dB bandwidth of 1.93 GHz, which matches well with the 3 dB bandwidth of the notch of the MDR and an extinction ratio of 15 dB.

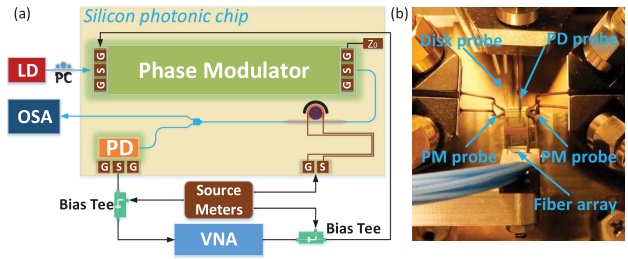

Fig. 4. (a) Schematic of the MPF experimental setup and (b) image of the fiber array and microwave probes setup captured by a camera.

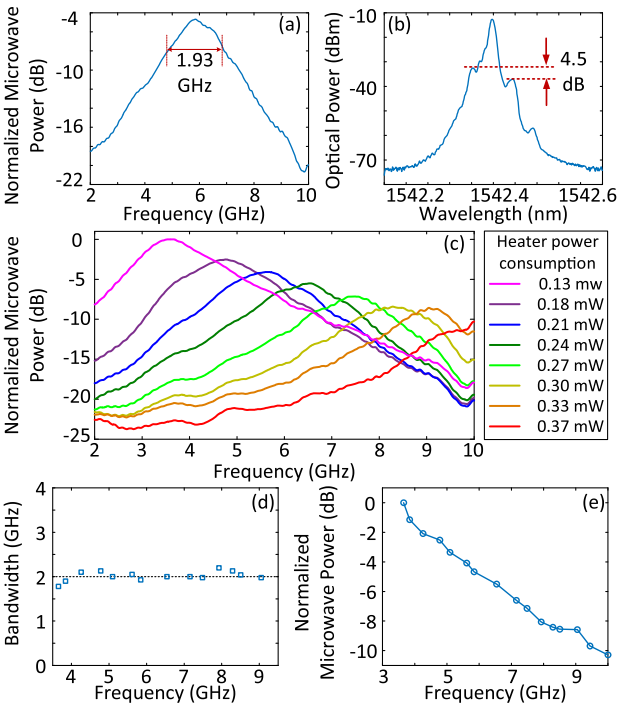

Fig. 5. (a) Frequency response of the MPF with a center frequency of 5.84 GHz, (b) optical spectrum of the modulated optical signal when the microwave signal frequency is 5.84 GHz, (c) measured frequency responses of the filter with the center frequency tuned from 3 to 10 GHz, (d) 3 dB bandwidth of the MPF when the center frequency is tuned from 3 to 9 GHz, and (e) microwave loss of the MPF with a center frequency tuned from 3 to 10 GHz.

Figure 5(b) shows the measured optical spectrum of the modulated optical signal at the output grating coupler when the incoming microwave signal frequency is 5.84 GHz. As can be seen, the lower first-order sideband power is higher than the upper one, which confirms that the phase-modulated double-sideband signal is converted to a single-sideband signal. Thus, the PM-IM conversion is achieved. The sideband suppression ratio could be further increased if the MDR has a high extinction ratio, which could be done by letting the MDR operate in the critical coupling condition through optimizing the coupling gap and length. Although the upper sideband is not completely suppressed, its residual power is very small, which still leads to an effective PM-IM conversion. By thermally tuning the MDR, the center wavelength of the notch is shifted, which causes the center frequency tuning of the MPF. Figure 4(c) shows the measured frequency responses of the MPF with the center frequency tuned from 3 to 10 GHz when a tunable DC voltage is applied to the micro-heater. As can be seen, a tuning range is as broad as 7 GHz achieved with a power consumption as small as 0.37 mW, which confirms the key advantage of the MPF in terms of a broad frequency-tunable range and low power consumption.

One added advantage of implementing an MPF based on PM-IM conversion is that the spectral shape is maintained when the center frequency of the passband is tuned. Figure 5(d) shows the 3 dB bandwidth of the MPF when the center frequency is tuned from 3 to 9 GHz. As can be seen, the 3 dB bandwidth of the realized MPF is maintained at around 2 GHz. Figure 5(e) shows the measured microwave loss when the center frequency is tuned from 3 to 9 GHz. The absolute loss when the MPF is operating at 3.58 GHz is 38.9 dB. In addition, the microwave loss is increased when the center frequency is tuned to a higher frequency. This is due to the unflat spectral responses of the PM and the PD.

In conclusion, we reported an on-chip frequency-tunable bandpass MPF implemented on a silicon photonic platform. Three key elements, including a high-speed PM, a thermally tunable high-Q MDR, and a high-speed PD were integrated on a single chip. The key element determining the spectral response of the MPF was the MDR, which was designed to have an additional slab waveguide to wrap the disk and the bus waveguide, to reduce the loss due to sidewall roughness. A bandpass MPF with a 3 dB bandwidth of 1.93 GHz, tunable from 3 to 10 GHz, was demonstrated. The power consumption was estimated to be 0.37 mW, which was considered to be low. The 3 dB bandwidth was maintained during the filter tuning, which was a key feature of an MPF implemented based on PM-IM conversion. The insertion loss of the MPF was also measured, which was 38.9 dB when the MPF was operating at 3.59 GHz. This successful implementation of an on-chip MPF marks a significant step forward in monolithical integration of microwave photonic subsystems and systems for low-cost and high-performance real-world applications.

Funding. Natural Sciences and Engineering Research Council of Canada (NSERC).

Acknowledgment. The authors acknowledge the CMC Microsystems for providing the design tools and enabling the chip fabrication.

REFERENCES

1. J. Yao, J. Lightwave Technol. **27**, 314 (2009).
2. R. A. Minasian, IEEE Trans. Microwave Theory Tech. **54**, 832 (2006).
3. J. Capmany, B. Ortega, and D. Pastor, J. Lightwave Technol. **24**, 201 (2006).
4. J. Yao, IEEE Microwave Mag. **16**(8), 46 (2015).
5. P. A. Morton and J. B. Khurgin, IEEE Photonics Technol. Lett. **21**, 1686 (2009).
6. X. Yi, T. X. H. Huang, and R. A. Minasian, IEEE Trans. Microwave Theory Tech. **58**, 3088 (2010).
7. J. Sancho, J. Bourderionnet, J. Lloret, S. Combrié, I. Gasulla, S. Xavier, S. Sales, P. Colman, G. Lehoucq, D. Dolfi, J. Capmany, and A. De Rossi, Nat. Commun. **3**, 1075 (2012).
8. D. Zhang, X. Feng, X. Li, K. Cui, F. Liu, and Y. Huang, J. Lightwave Technol. **31**, 3668 (2013).
9. W. Li, M. Li, and J. Yao, IEEE Trans. Microwave Theory Tech. **60**, 1287 (2012).
10. D. Marpaung, C. Roeloffzen, R. Heideman, A. Leinse, S. Sales, and J. Capmany, Laser Photonics Rev. **7**, 506 (2013).
11. J. S. Fandiño, P. Muñoz, D. Doménech, and J. Capmany, Nat. Photonics **11**, 124 (2017).
12. J. E. Bowers and A. Y. Liu, *Optical Fiber Communication Conference*, OSA Technical Digest (Optical Society of America, 2017), paper M2B.4.
13. B. Jalali and S. Fathpour, J. Lightwave Technol. **24**, 4600 (2006).
14. W. Zhang and J. Yao, *Optical Fiber Communication Conference*, OSA Technical Digest (Optical Society of America, 2018), paper M1 H.5.
15. W. Zhang and J. Yao, in *International Topical Meeting on Microwave Photonics (MWP)* (2017), pp. 1–4.
16. W. Zhang and J. Yao, J. Lightwave Technol., doi: 10.1109/JLT.2018.2829823.
17. W. Zhang and J. Yao, J. Lightwave Technol. **35**, 4418 (2017).